

**TRAJECTORY DESIGN FOR SMALL-SATELLITE MISSIONS  
TO NEAR-EARTH OBJECTS**  
IAA-LCPM-19-XX-XX

**Theodore H. Sweetser<sup>(1)</sup>, Rodney L. Anderson<sup>(2)</sup>, Gregory Lantoine<sup>(3)</sup>, Anastasios E. Petropoulos<sup>(4)</sup>, and Jon A. Sims<sup>(5)</sup>**

<sup>(1)(2)(3)(4)(5)</sup> *Jet Propulsion Laboratory, California Institute of Technology, 4800 Oak Grove Drive, Pasadena, CA, USA 91109, 1-818-354-4986, ted.sweetser@jpl.nasa.gov*

This paper describes new techniques for use in designing possible trajectories to near-Earth objects (NEOs) given the constraints imposed by the limited propulsive capabilities of small satellites and by being launched as a secondary with larger spacecraft. It illustrates the use of these techniques with the design of a trajectory that achieves rendezvous with the NEO 2007 UN12.

## INTRODUCTION

Small satellites offer significant cost savings for space missions, but they also offer considerable challenges to mission designers. The limited propulsive capabilities of small satellites and the fact that they are usually launched as secondary payloads with larger spacecraft into orbits unrelated to the small satellite mission impose serious constraints on the trajectory design. These constraints can only be met by the adoption of innovative design techniques at each stage of the trajectory. The first half of this paper describes these techniques and the remainder of the paper shows how their use dictates a design strategy that reverses the natural order—the design begins by determining the final stage of the trajectory, then finds the preceding stage that leads to it, and so on until the beginning of the trajectory is defined last.

### Small satellite propulsion

Small satellites range in mass from a few kilograms to a few hundred kilograms. Cubesats are a standard small spacecraft platform on the low end of that mass range. The basic building block size of a cubesat is 10 cm x 10 cm x 10 cm. This basic size is designated 1U. Cubesats can be composed of multiple 1U building blocks. The typical cubesat size is 1-6U, but even larger ones (e.g., 12U) are possible. Some basic rules of thumb for mass and power for cubesats include

- Mass: 1-2 kg per 1U unit
- Power: on the order of 100W for a 6U cubesat with 2 foldout solar arrays

These parameters are important for determining potential thrust accelerations for various combinations of cubesat size and thruster types (thrust and  $I_{sp}$ ).

In principle, any desired  $\Delta V$  can be achieved by a small satellite by making the mass fraction of propellant large enough. In practice the achievable  $\Delta V$  is limited by two factors. Firstly, in larger satellites it is relatively easy to increase the mass fraction of

propellant by increasing the size of the spacecraft (in particular its tanks) to allow additional propellant to be loaded; in small satellites, and especially in cubesats, this is not an option or at best a limited one. Secondly, the space needed for other subsystems such as telecom, attitude control, and command and data handling is relatively large; this will undoubtedly improve in the future.

Many standard propulsion options are available that are appropriate for spacecraft with masses of a few tens of kilograms and higher. For smaller spacecraft, like cubesats, the flight-proven propulsion options are very limited. Most cubesats launched up to now have had no primary propulsion system; however, many cubesats currently under development or being proposed, especially for missions beyond low to medium Earth orbit, now include a primary propulsion system. A wide variety of propulsion options are being considered, at a range of technology readiness levels (TRLs), including cold gas, warm gas, monopropellant, bipropellant, electrothermal, electrostatic, electromagnetic, solids, and propellantless (e.g., tethers and sails). The specific impulse for the propellant options ranges from about 50 sec for a cold gas system to several thousand seconds for some of the electric propulsion options. A report by the Committee on Achieving Science Goals with Cubesats gives an overview of current status and future direction for the technology development of propulsion options for cubesats. The report includes a table with some details on propulsion options for cubesats and their technical maturity to date.<sup>1</sup>

NASA has been and is funding development of many propulsion systems through the Space Technology Mission Directorate (STMD) Game Changing Development and Small Spacecraft Technology Program (SSTP). The charter for SSTP is to develop and mature technologies to enhance and expand the capabilities of small spacecraft, with propulsion being a particular focus. NASA's Pathfinder Technology Demonstrator (PTD) project, funded through SSTP, will demonstrate the operation of novel cubesat subsystem technologies on orbit, including propulsion. A demonstration mission for an iodine Hall thruster is being developed; the launch was most recently planned for mid-2018 but has been delayed pending further maturation of the propulsion system. Several cubesats slated to launch on EM-1, currently scheduled for late 2021, include primary propulsion systems. Example missions include NEA Scout (solar sail), Lunar Flashlight (was solar sail, now planning to use chemical), Lunar IceCube (iodine ion propulsion from Busek), and LunaH-Map (Busek warm gas and resistojet propulsion).

A rough initial scoping of the propulsive capabilities gives an upper limit of about 800 m/s velocity change (characteristic  $\Delta V$ ) using chemical propulsion and about 2000 m/s characteristic  $\Delta V$  using low-thrust, but we also consider trajectories requiring up to 50% more capability in order to identify particularly valuable new missions and to allow for future improvements in capability.

### **An overview of small satellite mission possibilities**

We assume that the initial state is either in GTO, GEO (geosynchronous Earth orbit), or on an hyperbolic or nearly-hyperbolic escape trajectory from Earth, since being left in low-Earth orbit requires at least 3 km/s impulsive  $\Delta V$ , or twice that using low thrust, in order to reach as far as the Moon. Since being carried as a secondary on an escape trajectory pretty much dictates a small satellite's destination, we consider in this paper only GTO and GEO orbits as starting conditions. These have been discussed in the context of lunar cubesat missions by Folta *et al.*<sup>2</sup> We will use them as starting points for trajectories that lead to deep space missions.

In many cases trajectories will be enabled by using lunar flybys and / or by exploiting the nonlinear dynamics of the Sun-Earth-Moon system to reduce the propulsive demands on the spacecraft. In any case a substantial  $\Delta V$  is needed to get started, even just to reach as far as the Moon. The Moon's distance can vary by as much as 50000 km, but this has a surprisingly small effect on the  $\Delta V$  needed to reach it. Based on Earth-centered conics it takes an impulse between 706 m/s and 718 m/s to reach the Moon from the periapse of a geosynchronous transfer orbit (GTO). From a geosynchronous orbit itself it takes more, between 1076 m/s and 1103 m/s.

The first "destination" we find past the Moon's orbit is the Earth-Sun Lagrange point  $L_2$ , or more generally libration orbits around it (also called Lagrange point orbits). Focusing on the periapse of the GTO we find that we need to increase the to-the-Moon impulse by between 72 m/s and 60 m/s to get out to the near edge of a libration orbit. It only takes another 27 m/s to reach escape velocity which is 11.021 km/s at an altitude of 185 km. Then to achieve a  $C_3$  of  $9 \text{ km}^2/\text{s}^2$  (appropriate for transfers to Mars or Venus) we need another 400 m/s, for a total of about 1200 m/s. This puts even the nearest planets out of reach of chemical-propelled small satellites in GTO.

That leaves us with Sun-Earth libration orbits, Earth-leading or -trailing heliocentric orbits, and transfers to NEOs. The following section examines different techniques that reduce the  $\Delta V$  needed for these closely related trajectories.

## **TECHNIQUES FOR DESIGNING TRAJECTORIES WITH CONSTRAINED PROPULSION**

We divide the process up into parts: low-thrust spiraling out for departure, multiple lunar flybys to maximize use of lunar gravity assists to increase energy and match departure time and direction, and use of stable and unstable manifolds associated with Sun-Earth libration orbits, which take advantage of Sun-Earth three-body dynamics to further reduce propulsive  $\Delta V$  requirements.

### **The uses of low thrust**

Electric propulsion (EP) offers a very mass-efficient means of escaping from an initial orbit around the Earth. The drawback of long flight times can be alleviated by using an initial impulse from a chemical propulsion system, but at a significant cost in terms of total propellant mass required. For example, an EP system with 8 microgees of acceleration can escape from low-earth orbit in about 3.5 years with a propellant mass fraction of about 0.2 ( $\Delta V \sim 6700 \text{ m/s}$  for  $3000 \text{ s } I_{sp}$ ); however, performing instead a 1-year hybrid escape, the required propellant mass fraction is 0.6, which leaves little room for flight system and payload mass. Escaping from GTO requires a propellant mass fraction of about 0.11 ( $\Delta V \sim 3400 \text{ m/s}$ ). We also find that the propellant mass fraction needed for spiral escape is most strongly affected by the initial semi-major axis, with eccentricity having only a minor effect. A slight initial eccentricity (about 0.05) confers a very small advantage, while eccentricity larger than about 0.3 confers a small disadvantage. Results are displayed graphically in Figure 1, which assumes an  $I_{sp}$  of 3000 s.

For low-thrust escape, flight time is often a driving factor. Thus we consider minimum-time low-thrust escape trajectories that are augmented with impulsive chemical maneuvers. First, minimum-time escape spirals, starting from a continuum of initial orbits that include LEO, GTO and GEO, are assessed in terms of the required low-thrust propellant mass fraction. This propellant mass fraction is applicable for thrust-to-

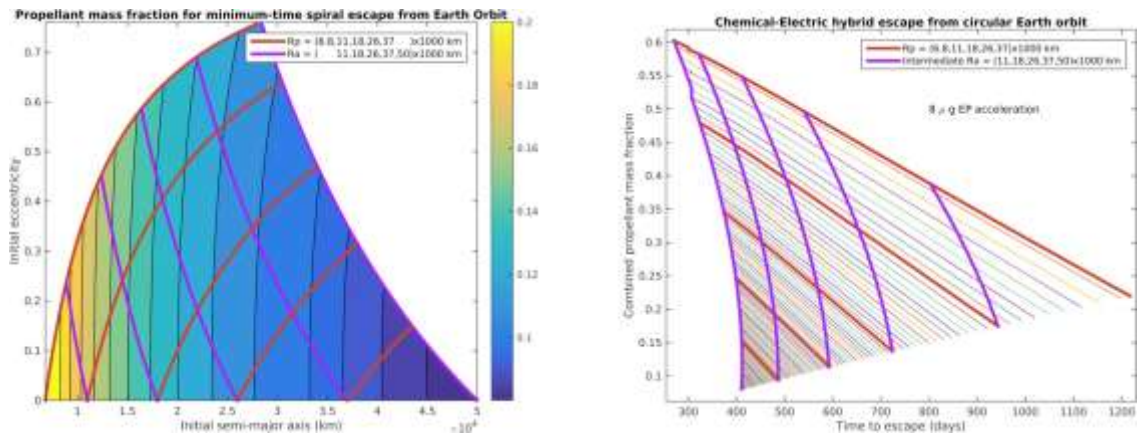


**Figure 1:** Propellant mass fraction for electric-propulsion or chemical-electric escape from various Earth orbits.

weight ratios less than about 0.01 and  $I_{sp}$  greater than about 1500s, a regime that easily encompasses most low-thrust, earth-orbiting systems. Second, hybrid escape trajectories significantly reduce flight time but only at a large propellant mass cost. Using plots like the ones shown in Figure 1, designers can rapidly size the propulsive requirements for various initial orbits to perform mission design trades.

Starting from GEO Offers the advantage of having multiple directions available, and takes substantially less  $\Delta V$  than from LEO, but has the disadvantage of being harder to hitch a ride.

Starting from GTO Offers the advantage of being easier to hitch a ride, has only a  $\sim 30\%$  penalty in  $\Delta V$  and TOF compared to GEO, but has the disadvantage of a less flexible departure orientation.

Some missions need only reach a manifold of a libration orbit, rather than a full escape condition, and therefore need less  $\Delta V$ . Such a case is examined later in the paper.

### The uses of lunar gravity assists

In general, small satellite missions to Near Earth Objects (NEOs) must have positive hyperbolic escape energies ( $C_3$ , in  $\text{km}^2/\text{s}^2$ ). A  $C_3$  above 2 is required for many NEO targets<sup>[3]</sup>. However, small satellite missions cannot afford a dedicated launch, and the launch  $C_3$  for secondary payloads is at most  $-2 \text{ km}^2/\text{s}^2$  for direct launches to the Moon (such as the upcoming EM-1 mission<sup>[4]</sup>). The difference in perigee velocity between a  $C_3$  of  $2 \text{ km}^2/\text{s}^2$  and a  $C_3$  of  $-2 \text{ km}^2/\text{s}^2$  is  $\sim 182 \text{ m/s}$ . To save that  $\Delta V$  and valuable propellant mass, multiple lunar flybys can be used to naturally increase the spacecraft hyperbolic escape velocity. In addition, solar perturbations between two lunar flybys can be used to provide an intermediate  $\Delta V$  for free around apogee to increase the lunar relative velocity ( $V$ ) and produce even higher escape energies.

The ability to easily design long lunar flyby sequences exploiting solar gravitational forces would therefore benefit many small satellite missions to NEOs. In particular, one critical building block of a long lunar flyby sequence is the associated solar-perturbed Moon-to-Moon transfer connecting two lunar flybys. In this task, to facilitate the design of long lunar flyby sequences, ballistic families of solar-perturbed Moon-to-Moon transfers are pre-computed in the Sun-Earth circular restricted three-body problem (CR3BP) and classified. Each family corresponds to a different number of months between lunar encounters. The families are parameterized by the initial lunar relative velocity and the solar phase angle (angle between the first lunar flyby location and the

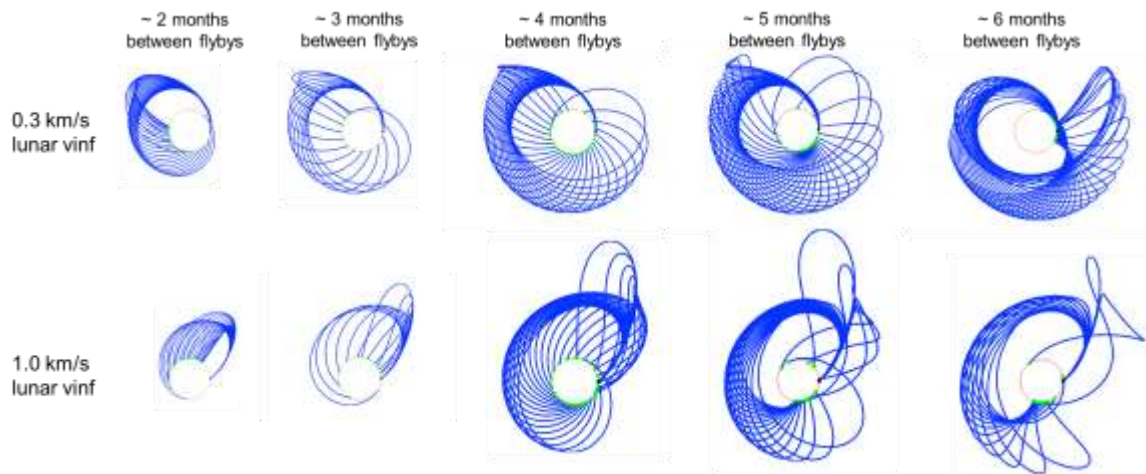


**Figure 2:** Complete families of solar-perturbed Moon-to-Moon transfers.

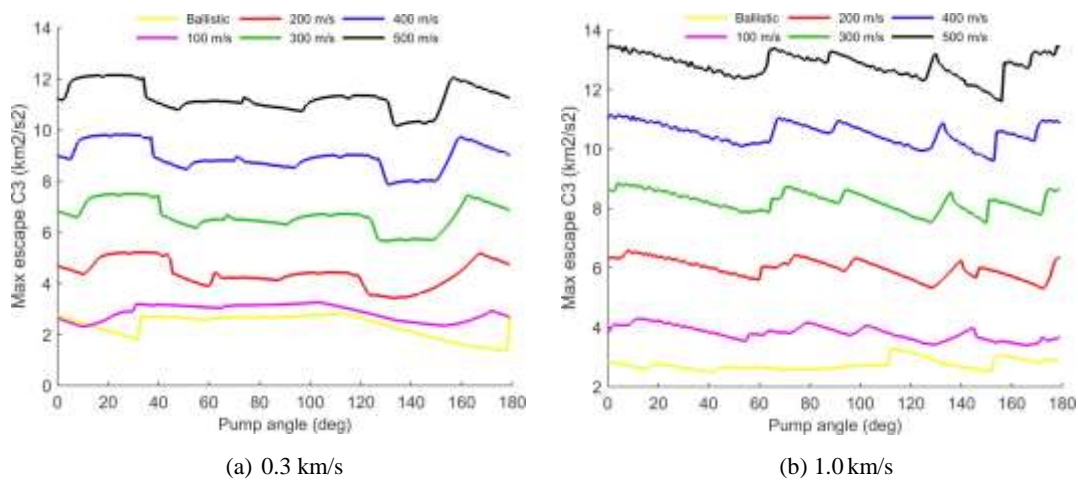


**Figure 3:** Maximum escape  $C_3$  vs pump angle for all solar-perturbed double lunar flyby sequences.

solar direction). The datasets associated with the families are then stored in a database. Family examples with initial lunar relative velocities of about 0.3 km/s (departure from GEO) and about 1.0 km/s (direct launch to the Moon or departure from GTO) are given in Figure 2.

The database can allow mission designers to quickly explore the trajectory space and choose appropriate trajectories for specific missions. In particular, in this task, for all family members, the turn angle of the final lunar flyby is varied to span the complete range of possible escape directions and energies. It is then possible to retrieve the maximum escape  $C_3$  vs. pump angle of the outbound asymptote with respect to the Earth's velocity vector. Of particular interest is the 0-degree pump escape direction, which corresponds to effective near-Hohmann transfers to NEOs. Applying a  $\Delta V$  at perigee is also considered to increase the escape  $C_3$  even further. The maximum achievable escape  $C_3$  vs. pump angle is shown in Figure 3 for different initial lunar relative velocities and increasing  $\Delta V$  magnitudes. As shown in Figure 3, solar-perturbed double lunar flyby sequences can increase the escape  $C_3$  to about 3 km<sup>2</sup>/s<sup>2</sup> when ballistic. When combined with perigee burns of a few hundreds of m/s, the escape  $C_3$  can be increased to 10 or more. In any case, this technique is promising for small satellite missions to NEOs.

## The uses of low-energy trajectories

NEOs of interest often tend to exist within the energy regime corresponding to those trajectories computed under the umbrella of low-energy trajectories. The link between Sun-Earth libration point orbit invariant manifolds and certain classes of NEOs was explored within the context of designing trajectories to NEOs by Lathrop and Anderson in 2010.<sup>[5]</sup> Sanchez and McInnes then examined the reverse problem, enabled by symmetries in the CR3BP, of bringing an asteroid back to the Earth-Moon system using the invariant manifolds of these types of orbits.<sup>[6]</sup> Others have also explored this scenario using various methods,<sup>7-10</sup> and the ARM mission was focused on returning to the Earth-Moon region from an asteroid.<sup>[11]</sup>

Anderson also explored trajectory options to NEOs by focusing on using planar orbits as initial guesses, and showed that many of the NEOs desirable for missions to asteroids are the same as those for bringing an asteroid back to the Earth-Moon system.<sup>[12]</sup> The following NEOs were identified as candidates for small-satellite missions: 1991 VG, 2000 SG344, 2006 QQ56, 2006 RH120, 2007 UN12, 2008 EL68, 2008 HU4, 2008 UA202, 2009 BD, 2010 JW34, 2010 UE51, 2010 VQ98, 2011 MD, 2011 UD21, 2012 TF79, and 2013 RZ53. A particular impulsive trajectory traveling to 2007 UN12 from a low-Earth orbit was explored in detail in that study. The invariant manifolds of libration point orbits may be used to enable transfers from GEO radius both in the plane and in three dimensions, and that is the focus of this analysis.

The equations of motion of a spacecraft in the circular restricted three-body problem in the rotating frame are

$$\begin{aligned}\ddot{x} - 2\dot{y} &= \frac{\partial \Omega}{\partial x} \\ \ddot{y} + 2\dot{x} &= \frac{\partial \Omega}{\partial y} \\ \ddot{z} &= \frac{\partial \Omega}{\partial z}\end{aligned}\tag{1}$$

where

$$\Omega = \frac{x^2 + y^2}{2} + \frac{(1 - \mu)}{r_1} + \frac{\mu}{r_2}.\tag{2}$$

Here,  $\mu$  is the mass of the smaller body (the secondary), and the mass of the larger body (the primary) is  $1 - \mu$ . The distances from the spacecraft to the primary and secondary, respectively, are

$$r_1 = \sqrt{(x + \mu)^2 + y^2 + z^2}, r_2 = \sqrt{(x - 1 + \mu)^2 + y^2 + z^2}.\tag{3}$$

The Jacobi constant is defined by

$$C = x^2 + y^2 + \frac{2(1 - \mu)}{r_1} + \frac{2\mu}{r_2} - \dot{x}^2 - \dot{y}^2 - \dot{z}^2\tag{4}$$

Computing transfers from GEO to Libration Orbits Lagrange point orbits and corresponding invariant manifolds at libration orbit gateways have been found to be useful for searching for pathways to and from asteroid trajectories. For missions traveling to asteroids, the Lagrange point orbits may serve as useful waypoints where the spacecraft may loiter or depart directly on an unstable manifold. The computations in general may be divided into two primary components: stable manifold transfers to

the libration point orbit, and unstable manifold transfers from the orbit to the asteroid.

Multiple orbits and options exist for computing low-energy transfers from orbits around the Earth to libration points orbits and on to asteroid rendezvous. As previously mentioned, Lathrop and Anderson,<sup>5</sup> and Anderson<sup>12</sup> explored cases traveling from low-Earth orbit (LEO) to libration point orbits. These studies focused on the planar cases as they were found to serve as a good basis for computing both planar and spatial trajectories. This analysis is extended here to examine transfers from the GEO radius, and three-dimensional orbits are also considered as an additional option for improving the initial guess for particular cases.

Lyapunov Orbit Transfers The stable manifold of a Lagrange point orbit may be used to transfer directly from LEO or GEO to the orbit. Sample transfers to both planar Lyapunov and 3D halo orbits were computed from GEO. The range of energies for each orbit family vary, with the planar Lyapunov orbit possessing a greater range.

The Lyapunov orbit family may be searched for orbits possessing a stable manifold  $W^S$  that just grazes the GEO radius, and the corresponding trajectory on that  $W^S$  that grazes this radius may be computed. This case is shown in Figure 4, and it corresponds to the orbit with  $C = 3.00086091204864$ . This is the minimum energy at which the stable manifold of the Lyapunov orbit reaches the GEO radius. For transfers to the  $L_2$  Lyapunov orbit from GEO, flight times of 7-8 months are realistic with  $\Delta V$ s of 1198-1216 m/s. Note that the trajectory will reach the vicinity of the Lyapunov orbit earlier, and a significant portion of this time is spent winding asymptotically onto the Lyapunov orbit.

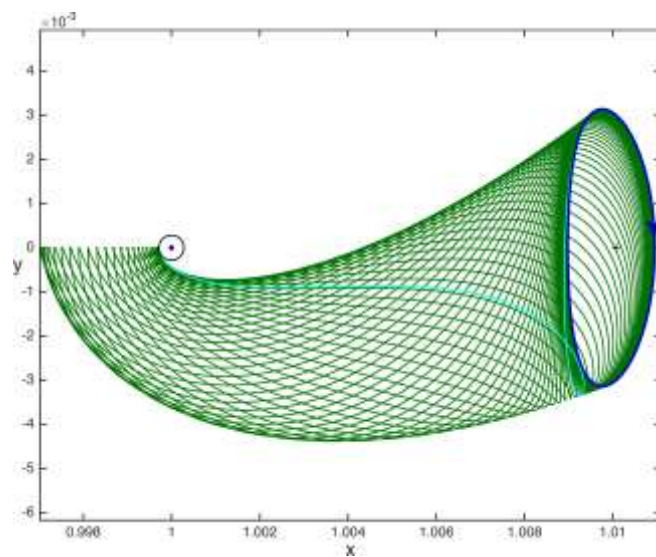
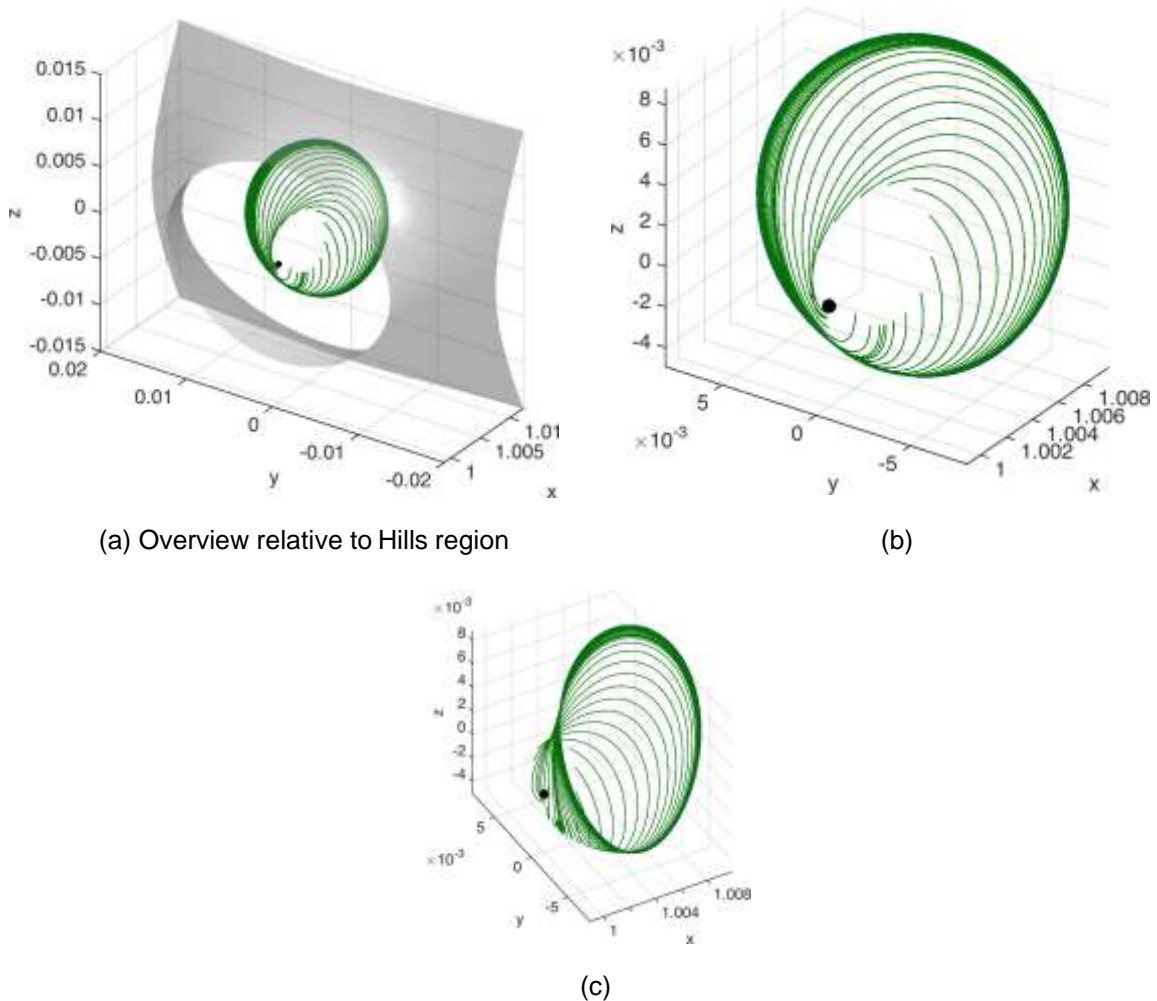


**Figure 4:** Lyapunov orbit and  $W^S$  generated at the Jacobi constant where the invariant manifolds just graze the GEO radius. The trajectory on the  $W^S$  that travels from the GEO radius to the Lyapunov orbit is shown in cyan.

Halo Orbit Transfers Lyapunov orbits serve as excellent initial guesses to compute transfers to asteroids both in and out of the plane, partly because the range of energies over which they exist provide a broader range of initial guesses than halo orbits.<sup>12</sup> For this reason, they have been the focus of earlier studies, but halo orbits do provide a more natural means to achieve trajectories traveling to higher inclinations. Their advantages are explored here, particularly for transfers from GEO radius

Halo orbits may be computed across a range of Jacobi constants using continuation, and the  $W^S$  of each halo orbit may be computed to search for a specific Jacobi constant corresponding to the energy where the lowest  $W^S$  trajectory just reaches the GEO radius on the first pass near the Earth. Such a procedure was performed for the Sun-Earth/Moon system, and the corresponding Jacobi constant was determined to be  $C = 3.00045708315725$ . The resulting halo orbit and its invariant manifolds are plotted



(a) Overview relative to Hills region

(b)

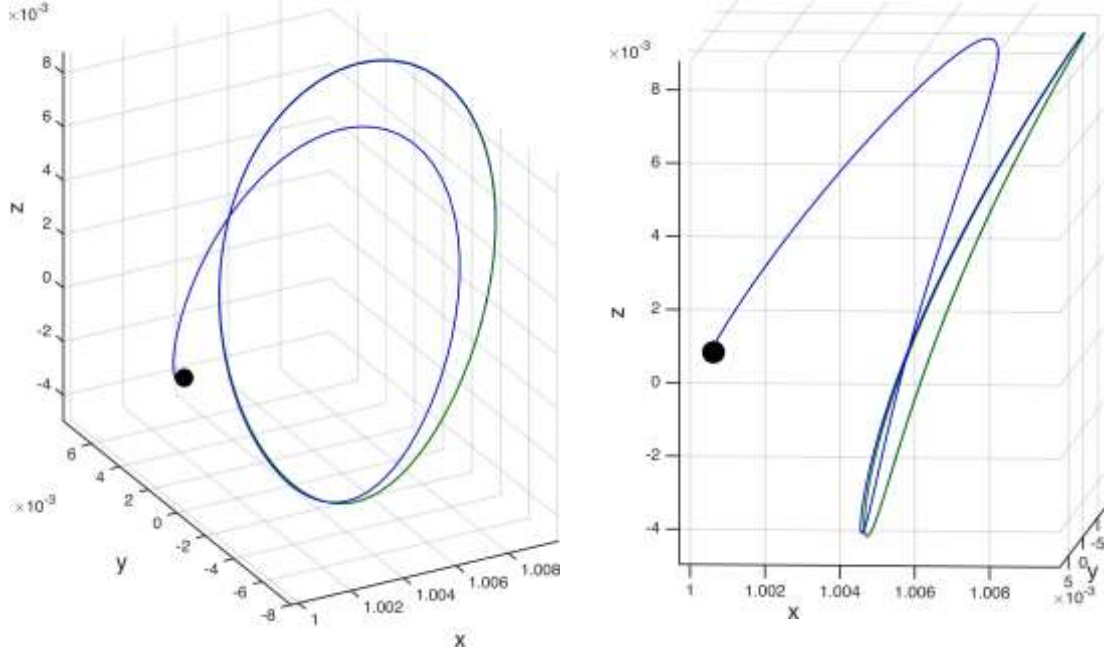
(c)

**Figure 5:** Stable manifold trajectories on halo orbit at energies where the trajectories just graze the GEO radius.

in Figure 5. The three-dimensional Hills region corresponding to the regions that are energetically inaccessible at this Jacobi constant is also plotted for reference. It can be seen that the halo orbit at this Jacobi constant has a significant vertical component that may enable the spacecraft to travel to a higher inclination more naturally than for the Lyapunov orbit cases. It is interesting that the  $C$  values obtained for the halo orbit case are less than for the Lyapunov case corresponding to higher energies, and this also provides additional options for launch from the Earth.

The specific trajectory on the invariant manifold that transfers from the GEO radius may be computed, and that resulting trajectory is given in Figure 6. In this case, the required  $\Delta V$  is approximately 1245 m/s, and the transfer duration is approximately 10.8 months. Again, the last portion of this trajectory is near the halo orbit, and is asymptotically winding onto the orbit.

Transfers on Halo Orbit  $W^u$  to Asteroids Libration point orbits provide a convenient location from which to search for low-energy transiting asteroids, and they also provide unstable manifold trajectory options traveling to these types of asteroids. The asteroid states are most easily accessed as orbital elements from JPL's Solar System Dynamics website, and for general rapid search schemes<sup>12</sup> it is most convenient to search for transfers on these invariant manifolds to these two-body trajectories.



(a) Overview

(b) Close view

**Figure 6:** Transfer to the  $L_2$  halo orbit from the GEO radius at  $C = 3.00045708315725$ .

However, this process using conic orbital elements is only valid where three-body effects are not significant. Specifically, the invariant manifold trajectories will generally be accurate even with close approaches to the secondary (the Earth/Moon barycenter), but the conic asteroid orbits will not be accurate if a close approach occurs. Given this constraint, potential rendezvous calculations are made here only outside the sphere of influence of the Earth/Moon barycenter given by

$$r_{soi} = \left(\frac{m_2}{m_1}\right)^{2/5} \rho \quad (5)$$

where  $\rho$  is the distance between the primary and the secondary. Inside this radius, the three-body effects become more significant.

Once the spacecraft travels on the stable manifold to the Lagrange point orbit, it may then depart from the Lagrange point orbit via its unstable manifold. These trajectories travel to both the exterior and interior regions of the CR3BP, and they may be searched for those that intersect with asteroid trajectories. Both trajectories leaving the Earth's region directly and those that fly by Earth are shown in Figures 7 and 8.

An idea of the three-body effects may be obtained by computing the semimajor axis  $a$  values as a function of the radius from the secondary ( $r_2$ ) as shown in Figure 9. Radii below the SOI radius are shown in the left in the gray region. Some variation in the semimajor axes are seen even above the SOI, and this is likely an effect from computing trajectories in this low-energy regime. The largest variations are seen below the  $r_{soi}$  as would be expected with close approaches of the secondary, and some variations at intermediate radii might be of interest for particular cases. In general, though, the orbital elements of the halo  $W^S$  appear to become more constant as the radius reaches approximately  $r = 0.02$  from the secondary. For general comparisons with the asteroid database in the following, the constant orbital elements of the  $W^S$

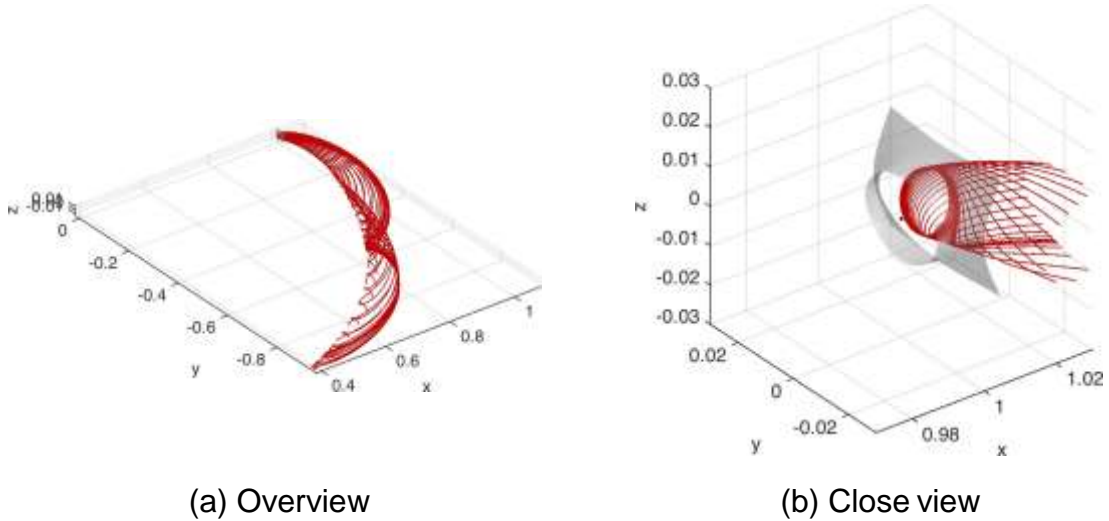


**Figure 7:**  $W^U$  of  $L_2$  halo orbit at  $C = 3.00045708315725$  computed for the sense corresponding to trajectories approaching the exterior region.

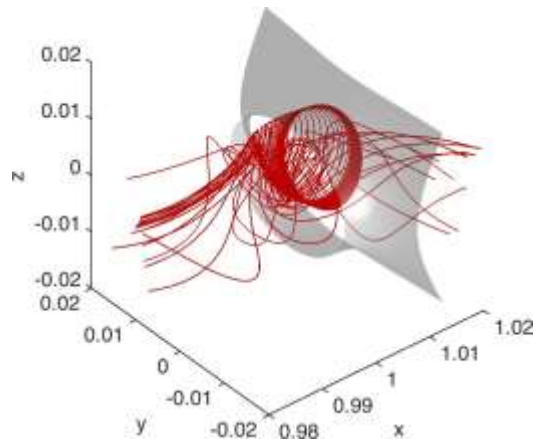


**Figure 8:**  $W^U$  of  $L_2$  halo orbit at  $C = 3.00045708315725$  computed for the sense corresponding to trajectories approaching the interior region.

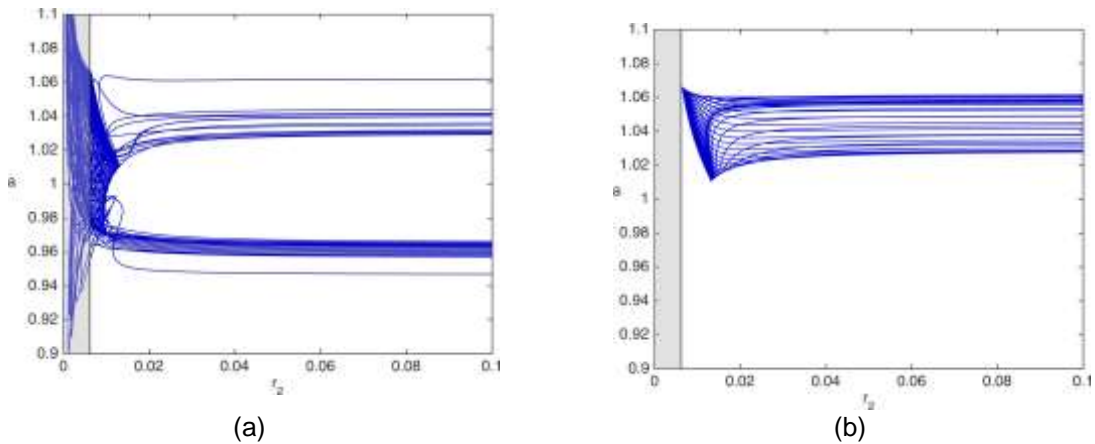


**Figure 9:** Semimajor axis  $a$  versus  $r_2$  for the  $L_2$  halo orbit  $W^S$  trajectories. (Left: includes flybys, and right: is the direct transfer to the exterior.)

trajectories are used. Generally, for smaller radii closer to the Earth/Moon barycenter, the effects of the Earth and Moon would need to be taken into account separately, and the three-body effects on the integrated asteroid trajectory are required to accurately analyze the problem in this case.

### Comparison to Asteroid Trajectories

A comparison of the orbital elements of the invariant manifolds outside of the sphere of influence with known asteroids may be made to aid in determining potential asteroids to target. A comparison at  $C = C_{geo}$  is shown in Figure 10. As might be expected, the majority of asteroids that have orbital elements near those of the invariant manifolds have a normalized semimajor axis near 1, and low eccentricities. A comparison with a broader range of  $C$  values is given in Figure 11.

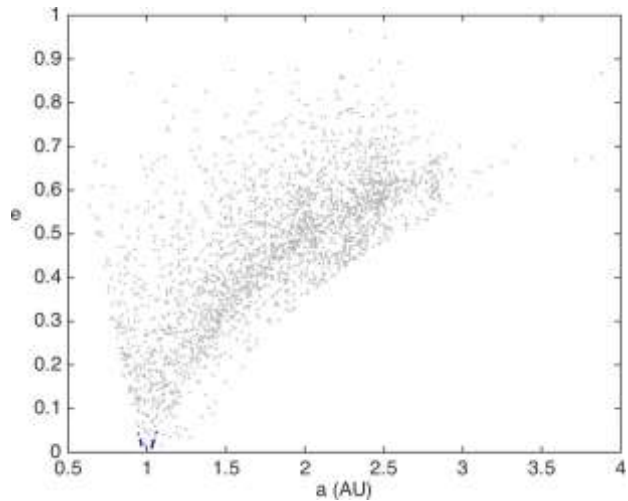


**Figure 10:** Comparison in  $a$  and  $e$  of  $W^U$  trajectories at  $C_{geo}$  to NEOs. Stable manifold orbits are shown in blue, and the asteroid orbital elements are in gray.

The same trends remain in semimajor axis and eccentricity, and it can be seen that most of the invariant manifolds remain near low inclinations, at least initially. Some of these inclination differences may be compensated for by using differential correction.

### **PUTTING IT TOGETHER—A SAMPLE MISSION TO ASTEROID 2007 UN12**

An excellent NEO target for a rendezvous is the Apollo-class asteroid 2007 UN12, because of its numerous close approaches to the Earth and its low inclination.

The choice of the propulsion system is critical for such a challenging mission. A traditional chemical system with low specific impulse ( $I_{sp}$ ) is likely to require a significant amount of propellant, which could be at odds with the low mass requirements of small satellites. Therefore, a low-thrust electric propulsion system with high  $I_{sp}$  is more suited for this mission and will require less propellant. Today, there exists already a large inventory of electric thrusters under development for small satellites.<sup>13–15</sup> In this study, four Microfluidic Electro spray (MEP) thrusters, under development at JPL,<sup>15</sup> are considered. Each thruster provides a maximum thrust of 0.2 mN at 5000 s  $I_{sp}$  and 8W of full input power. The spacecraft mass is assumed to be 14 kg (corresponding approximately to a 6U cubesat).

For planning purposes the mission will be divided into four phases: spiral orbit raising, Halo staging, lunar-powered escape, and interplanetary cruise. But the design actually is done back to front, starting with the interplanetary cruise to 2007 UN12, the start of which determines the end conditions of the lunar-powered escape with its two lunar gravity assists. Similarly, the design of each phase determines the end conditions of the preceding phase, which constrain its design in turn. In the following we discuss the phases of the full mission in the order they were designed.

#### **Interplanetary cruise**

MALTO (Mission Analysis Low Thrust Optimizer) was used to design the interplanetary cruise. MALTO is a preliminary low-thrust trajectory design tool that uses a series of impulsive burns to simulate continuous low-thrust trajectory arcs about a single gravitational body.<sup>16</sup> A known low-energy impulsive solution<sup>12</sup> is provided to MALTO as initial guess (excluding the loitering time in the Sun-Earth Halo orbit). The

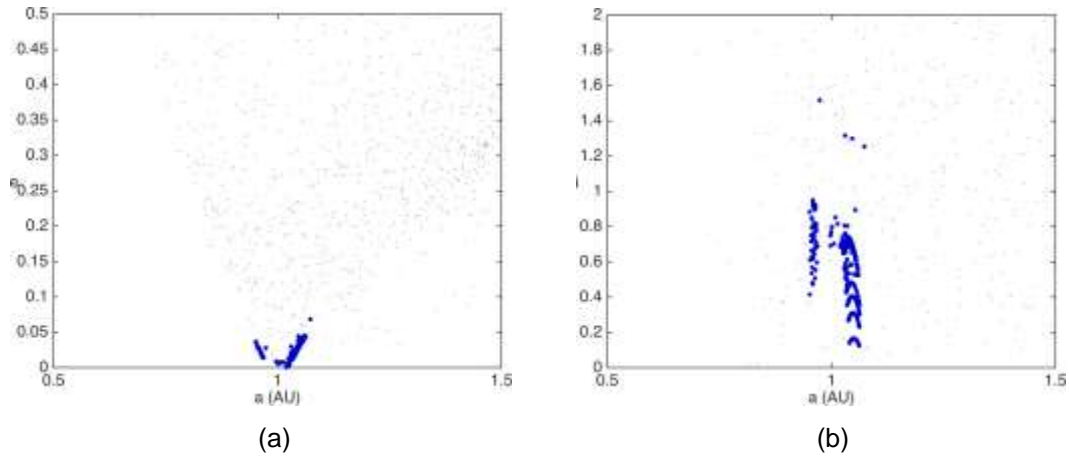


**Figure 11:** Comparison in  $a$  and  $e$  of  $W^U$  trajectories to NEOs across a range of  $C$ .

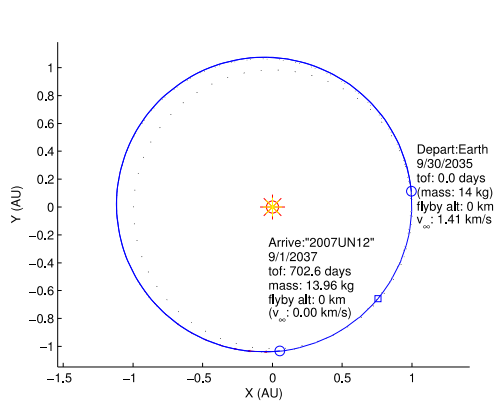


**Figure 12:** Interplanetary cruise trajectory in the ecliptic J2000 reference frame (Sun-centered).

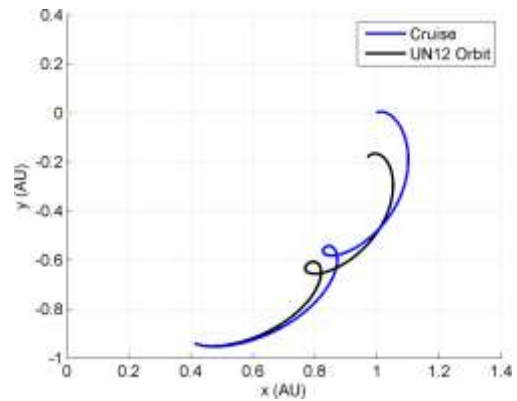


**Figure 13:** Interplanetary cruise trajectory in the Sun-Earth rotating frame (Sun-centered).

objective function is to maximize the spacecraft mass at asteroid arrival. Since a lunar escape is assumed, the escape  $C_3$  cannot exceed  $2 \text{ km}^2/\text{s}^2$  and the escape declination is capped to 30 deg (with respect to ecliptic). These upper bounds correspond to the maximum escape capability a double lunar flyby can provide.<sup>17</sup>

Thanks to the easy accessibility of the target, MALTO is able to find an efficient solution with 1.9 years flight time, 145 m/s  $\Delta V$  and only 40 g of propellant (see Figure 12). The launch occurs in September 2035 and the flight time is around 700 days. The  $\Delta V$  is lower than the impulsive solution because of the larger escape  $C_3$ . The spacecraft follows an Earth-trailing trajectory to rendezvous with 2007 UN12 (see Figure 13).

One potential challenge with this mission is the large Earth distance at which the rendezvous takes place (about 1.1 au, see Figure 14), placing high demands on the deep space communication system.

### Lunar escape

For spacecraft departing the Earth-Moon system, lunar flybys are beneficial and can significantly increase the hyperbolic escape energy ( $C_3$ , in  $\text{km}^2/\text{s}^2$ ) to about 2 for a modest increase in flight time of 3-6 months.<sup>17</sup> The optimal magnitude and direction

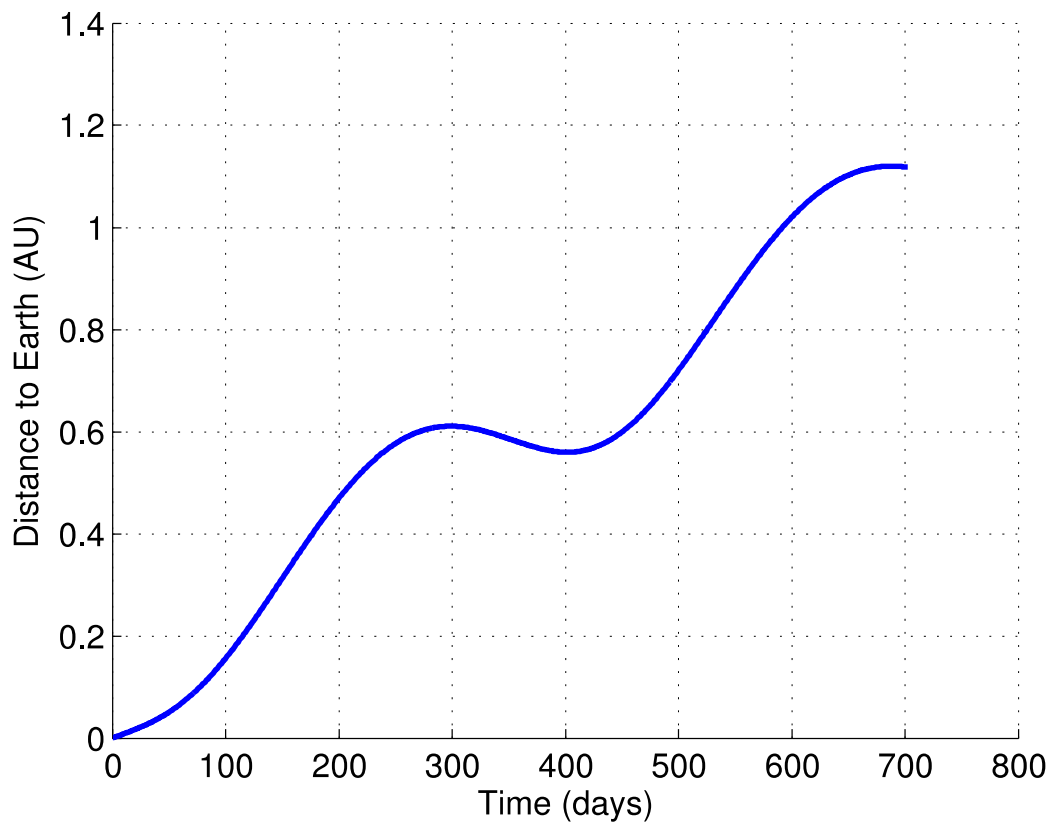


**Figure 14:** Distance to Earth as a function of flight time.

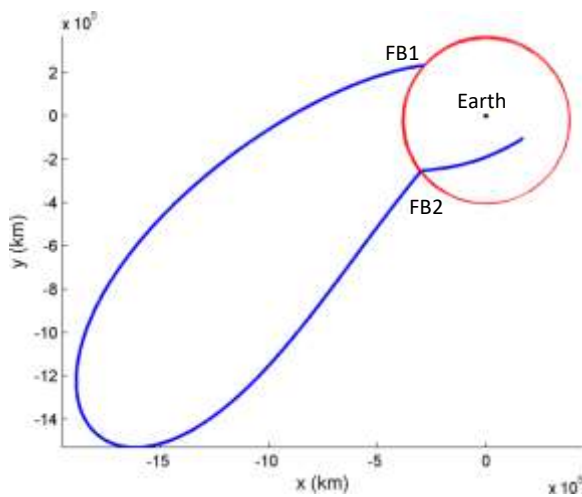


**Figure 15:** Lunar Escape trajectory in the ecliptic J2000 reference frame (Earth-centered).

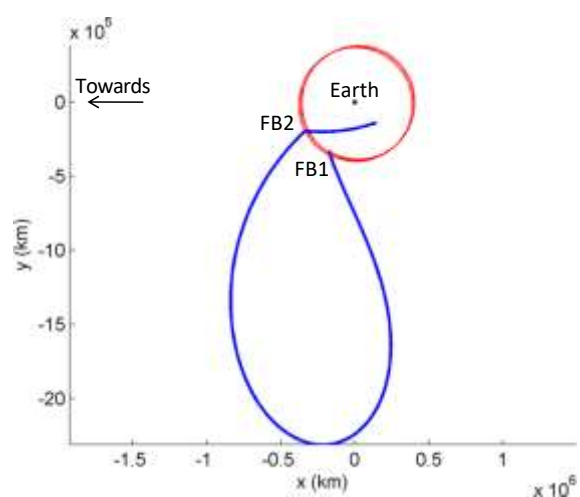


**Figure 16:** Lunar Escape trajectory in the Sun-Earth rotating frame (Earth-centered).

of the hyperbolic velocity vector is provided by the MALTO interplanetary solution. The database of Moon-to-Moon transfers (see Figure 2) is used to find a ballistic 4-month Double Lunar Flyby solution that matches exactly the Malto escape conditions (see Figure 15 and Figure 16). The first lunar flyby occurs on June 10, 2035 with a relative velocity of 0.9 km/s.

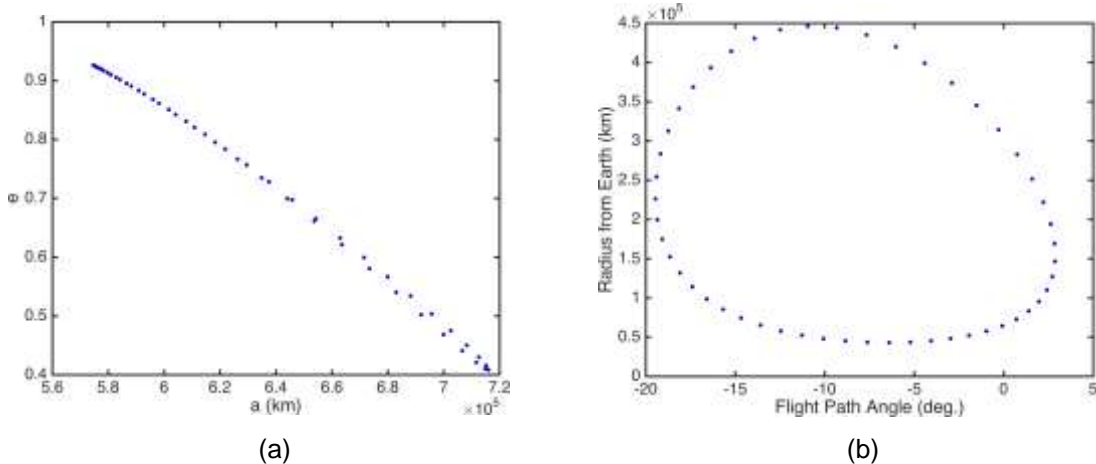


Figure 17: Initial conditions on the  $L_2 W^S$  to target at the end of the low-thrust spiral segment.

### Low-energy libration orbit staging phase

A low-thrust trajectory may be used for the first portion of the trajectory rather than targeting the initial conditions on the stable manifold of the Lyapunov orbit using impulsive maneuvers. In this case, for  $C = 3.00086091204864$ , the target initial states plotted in Figure 17 may be used. The corresponding target trajectories are shown in Figure 18.

Once the spacecraft transfers onto the stable manifold, it will continue impulsively to the Lyapunov orbit. It may either loiter at the  $L_2$  Lyapunov orbit, or, with minimal  $\Delta V$ , it may transfer onto the unstable manifold to travel back to the Moon. There it may begin a flyby sequence and transfer onto a low-thrust trajectory for asteroid rendezvous. The stable manifold transfer is shown in Figure 19.

### Low-thrust initial spiral phase

Starting in a GTO with the full initial mass of 14 kg, using a mere 1 kg of propellant, the spacecraft can spiral up to the starting conditions of one of the stable manifolds shown in Figures 17 and 18. In particular, we target a semimajor axis of

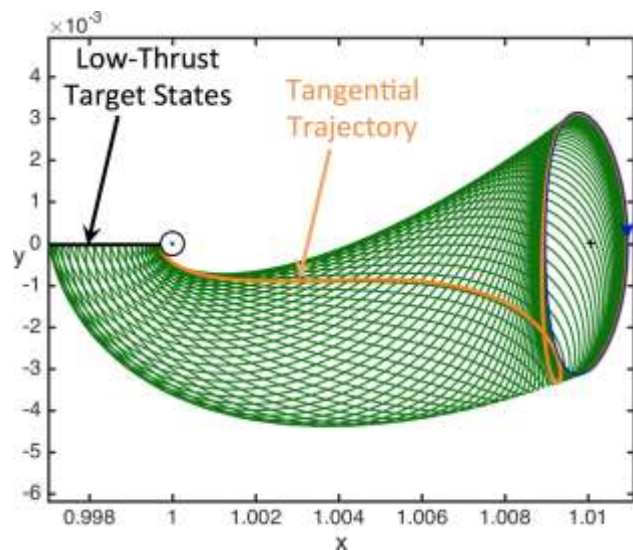


Figure 18: Trajectories on the  $L_2 W^S$  to target at the end of the low-thrust spiral segment.

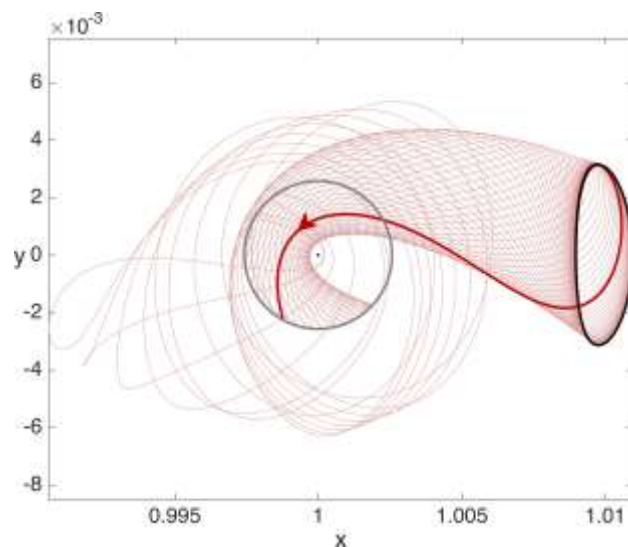
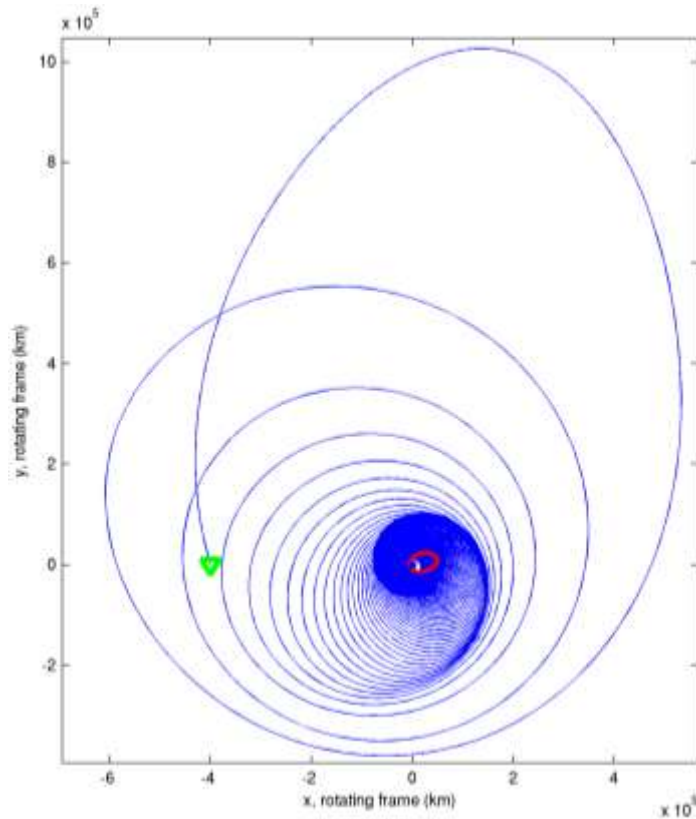


Figure 19: Lyapunov stable manifold transfer to the Moon at  $C = 3.00086091204864$ .



**Figure 20:** Spiral transfer from GTO to a stable manifold.

$6.96 \times 10^5$  km and eccentricity of 0.503 using the Q-law feedback control algorithm<sup>18</sup> for the thrust profile. The resulting spiral is shown in Figure 20 in the rotating frame. The flight time on the spiral is about 650 days.

## CONCLUSION

With the stages of the trajectory now defined piecemeal, we wind them up to describe the complete trajectory. The spacecraft begins in a GTO orbit and uses low thrust to spiral out to attain a semi-major axis and eccentricity matching a point on a stable manifold leading to a Sun-Earth  $L_2$  Lyapunov orbit. Once in the  $L_2$  Lyapunov orbit a properly timed minimal  $\Delta V$  puts the spacecraft on an unstable manifold leaving the  $L_2$  Lyapunov orbit and going to a close approach to the Moon. Beginning with that close approach a series of lunar flybys increases the geocentric  $C_3$  of the spacecraft to about  $2 \text{ km}^2/\text{s}^2$  and lines it up with the beginning of an optimal low-thrust transfer to 2007 UN12. The entire trajectory requires 1.04 kg of propellant for the low-thrust propulsion system.

The techniques described in this paper, in particular the database of Moon-to-Moon transfers, are now being applied in the design of the Lunar Flashlight and Near-Earth Asteroid Scout missions.

## ACKNOWLEDGMENT

The work described in this paper was carried out in part at the Jet Propulsion Laboratory, California Institute of Technology, under a contract with the National Aeronautics and Space Administration.

## REFERENCES

- [1] National Academies of Sciences, Engineering, and Medicine, *Achieving Science with CubeSats: Thinking Inside the Box*. Washington, DC: The National Academies Press, 2016, doi:10.17226/23503.
- [2] D. Folta, D. Dichmann, P. Clark, A. Haapala, and K. Howell, "Lunar Cube Transfer Trajectory Options," *AAS/AIAA Space Flight Mechanics Meeting*, No. AAS 15-353, Williamsburg, Virginia, January 11–15, 2015.
- [3] E. Asphaug, "Planetary Science Decadal Survey Near Earth Asteroid Trajectory Opportunities in 2020–2024", NASA tech document, 2010.
- [4] C. Blackerby and H. C. Cate, "The Space Launch System: NASA's Exploration Rocket," *29th International Symposium on Space Technology and Science*, Nagoya-Aichi, Japan, 2-9 June 2013.
- [5] B. W. Lathrop and R. L. Anderson, "Survey of  $\Delta V$  Requirements for Low Energy Transfers to Near Earth Objects," *AAS George H. Born Astrodynamics Symposium*, Boulder, CO, May 13-14 2010.
- [6] J. P. Sanchez and C. R. McInnes, "On the Ballistic Capture of Asteroids for Resource Utilisation," *62nd International Astronautical Congress*, No. IAC-11.C1.4.6, Cape Town, South Africa, 2011.
- [7] J. Brophy, F. Culick, and L. F. e. al., "Asteroid Retrieval Feasibility Study," tech. rep., Keck Institute for Space Studies, California Institute of Capturing Technology, Jet Propulsion Laboratory, Pasadena, California, April 2 2012.
- [8] N. Lladó, Y. Ren, J. J. Masdemont, and G. Gómez, "Capturing Small Asteroids Into Sun-Earth Lagrangian Points for Mining Purposes," *63rd International Astronautical Congress*, No. IAC-12.C1.6.7, Naples, Italy, October 1-5 2012.
- [9] D. García Yárnoz, J. P. Sanchez, and C. R. McInnes, "Easily Retrievable Objects Among the NEO Population," *Celestial Mechanics and Dynamical Astronomy*, Vol. 116, No. 4, 2013, pp. 367–388.
- [10] H. Baoyin, Y. Chen, and J. Li, "Capturing Near Earth Objects," *Research in Astronomy and Astrophysics (Chinese Journal of Astronomy and Astrophysics)*, Vol. 10, No. 6, 2010, pp. 587–598.
- [11] N. Strange, D. Landau, T. McElrath, G. Lantoine, T. Lam, M. McGuire, L. Burke, M. Martini, J. Dankanich, "Overview of Mission Design for NASA Asteroid Redirect Robotic Mission Concept," *33rd International Electric Propulsion Conference*, No. IEPC-2013-321, Washington, D.C., October 6-10, 2013.
- [12] R. L. Anderson, "A Quick Search Method for Low-Energy Trajectory Options to Near Earth Objects," *24th AAS/AIAA Space Flight Mechanics Meeting*, No. AAS 14-233, Santa Fe, New Mexico, January 26-30 2014.
- [13] M. Keidar, T. Zhuang, A. Shashurin, G. Teel, D. Chiu, J. Lukas, S. Haque, and L. Brieda, "Electric propulsion for small satellites," *Plasma Physics and Controlled Fusion*, Vol. 57, No. 1, 2015, p. 014005.
- [14] W. Wright and P. Ferrer, "Electric micropropulsion systems," *Progress in Aerospace Sciences*, Vol. 74, 2015, pp. 48–61.

- [15] C. M. Marrese-Reading, J. K. Ziemer, D. P. Scharf, T. Martin-Mur, J. Mueller, and R. E. Wirz, "Mission enabling and enhancing spacecraft capabilities with micro-newton electric propulsion," *Proceedings of the IEEE Aerospace Conference, Big Sky, MT*, 2010.
- [16] J. A. Sims *et al.*, "Implementation of a Low-Thrust Trajectory Optimization Algorithm for Preliminary Design," *AIAA/AAS Astrodynamics Specialist Conference*, Paper AIAA 2006-6746, 2006.
- [17] T. McElrath *et al.*, "Using Gravity Assists in the Earth-Moon System as a Gateway to the Solar System," *IAF/AIAA Global Space Exploration Conference*, Paper GLEX-2012.05.5.2x12358, 2012.
- [18] Petropoulos, A.E., "Refinements to the Q-Law for Low-Thrust Orbit Transfers," AAS Paper No. 05-162, AAS/AIAA Space Flight Mechanics Meeting, Copper Mountain, CO, Jan. 2005.